Structures 45 (2022) 2067–2079

Contents lists available at ScienceDirect

Structures

journal homepage: www.elsevier.com/locate/structures

Flexural behavior of reinforced concrete beams prepared with treated Wastewater, recycled concrete Aggregates, and fly ash

Abdelrahman Abushanab, Wael Alnahhal *

Department of Civil and Architectural Engineering, College of Engineering, Qatar University, Doha, Qatar

ARTICLE INFO

Keywords:
Sustainability
Treated wastewater
Recycled concrete aggregates
Fly ash
Reinforced concrete beams
Flexural behavior

ABSTRACT

Utilizing treated domestic wastewater (TWW), recycled concrete aggregates (RCA), and fly ash (FA) in reinforced concrete (RC) structures is of great interest from a sustainability perspective. In this study, four RC beams (180 × 250 × 2000 mm) were fabricated and tested under a four-point bend flexure until failure. The test parameters include mixing water type (fresh water and TWW), coarse aggregate type (natural gabbro and RCA), and FA content (0% and 20%). The results suggested that the use of TWW, RCA, and FA had no significant effect on the beams' cracking patterns and reinforcement strain at yielding, whereas TWW and RCA decreased the beams' ductility by 8.7% and 15.9%, respectively. In addition, TWW reduced the beams' flexural capacity by 13.7%. On the other hand, the use of FA increased the beams' cracking and ultimate loads and concrete maximum strain and negligibility increased the ductility. The analytical investigations revealed that the ACI 318–19 code accurately predicted the beams' cracking moments, while the CSA-A23.3–14 code showed the least prediction error for the beams' ultimate moments. Additionally, the CSA-A23.3–14 showed an accurate prediction of the beams' load–deflection responses.

1. Introduction

Major concerns have recently arisen about the worldwide overproduction of concrete and the consequent challenges for the global environment, economy, and natural resources. Concrete is currently the second most consumed material in the world, after water, with over nine billion tons produced annually. The substantial consumption of concrete has serious repercussions for the worldwide depletion of freshwater and natural aggregate (NA) resources. The concrete industry uses one trillion gallons of fresh water for concrete manufacturing alone, without considering concrete curing and washing processes. Moreover, demand for NA increased by 91% between 2007 and 2014 and is expected to jump by 215% by 2025. In addition, 10% of the total CO_2 exhaust in the environment is due to concrete applications. Consequently, there is a pressing need to incorporate recyclable materials into concrete applications [1–3].

Researchers have recently put forward achievable measures for replacing fresh water with treated domestic wastewater (TWW) in concrete applications [2,4–7]. Nonetheless, available research focused only on the material level of TWW concrete [2,6]. Asadollahfardi et al. [6] observed that TWW delayed the initial and final setting times of ordinary Portland cement (OPC) by 10 and 60 min, respectively, while TWW concrete had approximately similar mechanical characteristics to normal concrete. In addition, the authors studied the microstructure of TWW concrete and found that it is more porous than conventional concrete. More recently, Abushanab and Alnahhal [2] demonstrated that TWW concrete had a negligible decrease in concrete mechanical properties, whereas the durability properties were significantly dropped by about 40% with TWW.

On the other hand, some researchers have recommended utilizing recycled concrete aggregates (RCA) in reinforced concrete (RC) applications to compensate for the insufficiency of NA. Research on RCA has progressed greatly in plain and RC applications [1,8–10]. Hossain et al. [11] pointed out that incorporating RCA in concrete applications reduces greenhouse gas emissions and energy consumption by 65% and 58%, respectively. Wang et al. [9] noticed that recycled aggregate concrete (RAC) exhibited a 26% lower slump than natural aggregate concrete (NAC). The authors also observed that using 100% RCA in concrete decreased the compressive and flexural strengths by 40 to 45%. Moreover, Chen et al. [12] recorded a reduction of 11% in the compressive strength when 100% of coarse NA were replaced with RCA. Nevertheless, Alnahhal and Aljidda [13] found that RAC and NAC

* Corresponding author.
E-mail addresses: aa1104287@qu.edu.qa (A. Abushanab), wael.alnahhal@qu.edu.qa (W. Alnahhal).

https://doi.org/10.1016/j.istruc.2022.10.029
Received 26 May 2022; Received in revised form 26 August 2022; Accepted 5 October 2022
Available online 14 October 2022

Table 1
Chemical characteristics of fresh water and TWW.

Characteristic	Unit	Fresh water	TWW	QCS 2014 [22]	ASTM C1602 [23]	BS EN 1008:2002 [24]
Zinc (Zn^{+2})	mg/l	0.0046	0.1051	100	–	–
Iron (Fe^{+2})	mg/l	0.0135	0.077	–	–	–
pH	–	8.1	7.8	6.5–9.0	–	≥4
Chloride (Cl^{-})	mg/l	14.1	511		500 (PS elements) 1000 (RC elements) 4500 (PC elements)	500 (PS elements) 1000 (RC elements)
Chlorine (Cl_2)	mg/l	<0.1	<0.1	–	–	–
Sulfate (SO_4^{-2})	mg/l	6	490	2000	3000	2000
Dissolved oxygen	mg/l	9.4	8	–	–	–
Phosphate (PO_4)	mg/l	<0.03	9.19	–	–	–
Total suspended solids	mg/l	2	3	–	–	100
Total dissolved solids	mg/l	93	1690	2000	50,000	2000

Note: PS = prestress and PC = plain concrete.

exhibited comparable mechanical properties. More recently, Abushanab and Alnahhal [14] noticed that RAC-TWW mixes achieved higher mechanical properties than NAC-TWW mixes. Regarding the effect of RCA on the flexural behavior of RC beams, Choi and Yun [15] found that the flexural capacity of RAC-RC beams was 20% lower than that of NAC-RC beams. However, Alnahhal and Aljidda [13] revealed that the ultimate flexural strength of RAC-RC beams only decreased by 5 to 9%. The authors also pointed out that the failure mode of the beams was not affected by the aggregate type. Arezoumandi et al. [16], Kang et al. [17], and Seara-Paz et al. [18] recognized that RAC-RC beams exhibited closer crack spacing, a slightly lower cracking moment, and 5 to 22% higher deflection than NAC-RC beams.

As presented above, RAC's properties were found to be inferior when compared to NAC. Therefore, researchers have devised several methods to improve the characteristics of RAC; one method is to coat the surface of RCA with the by-product fly ash (FA) [19]. In their research, Lima et al. [19] found that the mechanical properties of FA-RAC at later ages were similar to those of NAC. Furthermore, the chloride permeability of RAC was significantly enhanced by partially replacing OPC with FA. Nevertheless, few investigations to date have evaluated the influence of FA on RAC-RC structural elements. Sunayana and Barai [20] observed that replacing 30% of OPC with FA in RAC-RC beams decreased the cracking moment by 30%. However, the yield and ultimate moments were comparable to NAC-RC beams. In addition, the flexural ductility of RAC-RC beams was enhanced by adding FA.

Although the above literature demonstrates the feasibility of using TWW, RCA, and FA for concrete applications, a significant research gap related to the effect of such a combination on the flexural behavior of RC beams remains. Thus far, no studies have been done on the flexural behavior of RC beams with TWW. In addition, very few studies have investigated the influence of FA on the flexural behavior of RAC-RC beams. Therefore, this study fills this gap in the existing literature by experimentally and analytically investigating the flexural capacity of RC beams simultaneously made with TWW, RCA, and FA.

2. Materials and methods

2.1. Materials

2.1.1. Mixing water

The concrete mixing water investigated was fresh water and TWW. The fresh water used is typically utilized for concrete manufacturing applications in Qatar. On the other hand, the TWW used was of tertiary TWW type and was supplied by a sewage treatment plant in Qatar. Table 1 includes the chemical characteristics of fresh water and TWW, which were evaluated according to the standard methods for the examination of water and wastewater [21]. The chemical characteristics of TWW and fresh water were as per the allowable limits for RC members as per Qatar Construction specification (QCS 2014 [22]), ASTM C1602 [23], and BS EN 1008:2002 [24] specifications. However, TWW is characterized by higher concentrations of chloride, zinc, total dissolved solids, phosphate, iron, and sulfate than fresh water.

Table 2
Physical characteristics of coarse aggregates and sand.

Property	GA	RCA	Sand	QCS 2014 [22]
Water Absorption (%)	0.72	3.51	0.6	2 (coarse NA) 3 (RCA) 2.3 (sand)
Soundness (%)	2.2	12.6	10.3	15
Elongation index (%)	24	8	—	35
Los Angeles Abrasion (%)	8.9	17.6	—	30
Flakiness index (%)	6.9	5.2	—	35
Dry Specific Gravity	2.89	2.47	2.62	—
SSD Specific Gravity	2.91	2.55	2.63	—
Apparent Specific Gravity	2.95	2.70	2.65	—

2.1.2. Coarse and fine aggregates

The investigation included two coarse aggregate types: gabbro aggregates (GA) and RCA. GA are a natural type of aggregates, whereas RCA were obtained from demolished concrete with a compressive strength of 50 MPa. Moreover, natural washed sand was used in all RC beams as fine aggregates. The physical properties and particle gradation of the coarse and fine aggregates are presented in Table 2 and Fig. 1, respectively. It could be seen that all properties of RCA, excluding the water absorption, were below the maximum limits specified by QCS-14 [22]. In principle, RCA had 388% and 17% higher water absorption than GA and QCS-14 [22] limits, respectively, owing to the adhered mortar of RCA. Furthermore, it could be observed from Fig. 1(b) that GA and RCA had approximately similar particle gradation and sizes (4.75 to 19 mm) and were within the specified limits of ASTM C33/C33M-18 provisions [25].

2.1.3. Cement, FA, and steel

Conventional OPC type I and class F FA with specific gravities of 3.15 and 2.18, respectively, were used as binders in this study. The particle size of OPC and FA ranges between 10 and 90 μm and 3 to 55 μm, respectively. The FA used had a moisture content of 0.5% according to ASTM C311/C311 M – 18 [26]. The binders' oxides were obtained using X-ray fluorescence (XRF) analysis and presented in Table 3. The XRF results showed that the amount of silica in FA is significantly higher than that of OPC, indicating a higher capacity for FA to react with $Ca(OH)_2$ hydrate to densify the cement matrix. In addition, all OPC and FA oxides were within the specified limits of ASTM C150/C150M–20 [27] and ASTM C618–19 [28], respectively. On the other hand, conventional steel bars of 8, 10, and 12 mm diameters were used. The mechanical specifications of steel reinforcement are shown in Table 4, as obtained from the manufacturer datasheet.

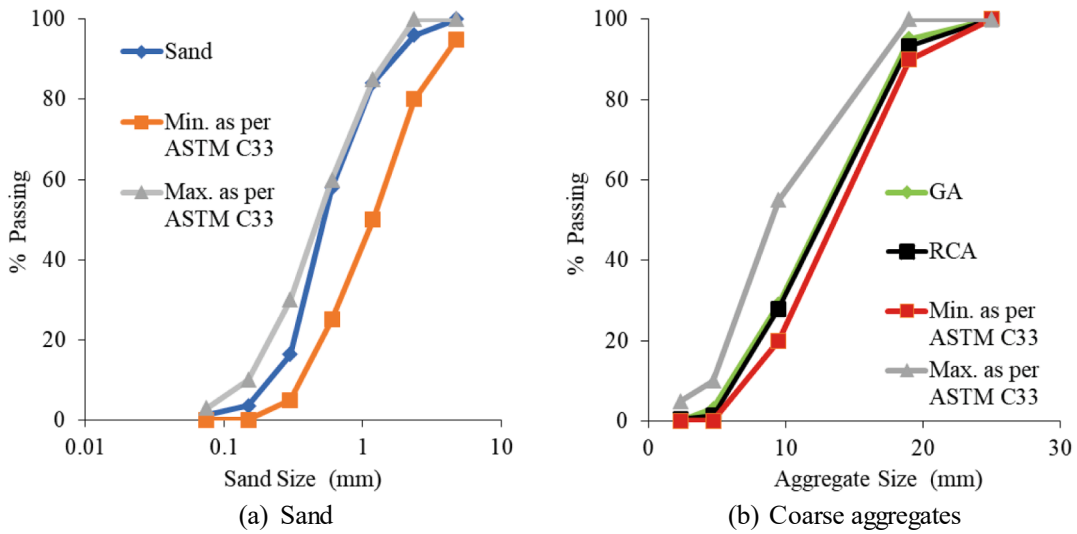

Fig. 1. Sieve analysis for sand and coarse aggregates used.

Table 3
OPC and FA oxides with ASTM C150/C150M–20 [27] and ASTM C618–19 [28] guidelines' limits.

Oxide (% weight)	OPC	ASTM C150/C150M – 20 [27]	FA	ASTM C618 – 19 [28]
Y_2O_3	–	–	0	–
ZrO_2	–	–	0.07	–
Nio	–	–	0.02	–
MgO	2.5	Maximum 5	1.57	–
Al_2O_3	3.48	Maximum 6	28.49	
SO_3	2.8	Maximum 3	0.51	Maximum 5
P_2O_5	–	–	0.62	–
Cr_2O_3	0.05	–	0.04	–
CL	0.05	–	0.12	–
K_2O	0.47	–	1	–
CaO	68.91	–	2.74	Maximum 18
MnO	0.09	–	0.09	–
V_2O_5	0.05	–	0.04	–
Na_2O	–	–	0.06	–
TiO_2	0.28	–	1.95	–
SiO_2	15.84	Minimum 20	55.97	Minimum 50*
SrO	0.05	–	0.06	–
Fe_2O_3	4.8	Maximum 6	6.63	

Note: * for SiO_2, Fe_2O_3, and Al_2O_3.

Table 4
Mechanical properties of steel reinforcement.

Bar diameter	Modulus of elasticity (GPa)	Yield tensile strength (MPa)	Yield strain (%)	Ultimate tensile strength (MPa)
8	191	512	0.268	551
10	193	515	0.267	555
12	194	519	0.268	553

2.2. Concrete mixes

As shown in Table 5, four concrete mixes were prepared in this study with a constant water-to-cement ratio of 0.45. Concrete mixes were labeled based on the investigated parameters. The first letter ('F' and 'T') refers to the type of mixing water as fresh water and TWW, respectively. The second letter ('G' and 'R') refers to the type of coarse aggregates as GA and RCA, respectively. The third letter refers to the type of binders used (O for 100% OPC and F for the blend of 80% OPC and 20% FA). Fresh water and GA were replaced completely by TWW and RCA,

Table 5
Concrete mix proportions.

Proportion (kg/m^3)	Mix			
	FGO	TGO	TRO	TRF
Fresh water	156.4	0	0	0
TWW	0	156.4	156.4	156.4
GA	1075.5	1075.5	0	0
RCA	0	0	942.4	942.4
Sand	708.1	708.1	708.1	708.1
OPC	349.2	349.2	349.2	279.3
FA	0	0	0	69.8

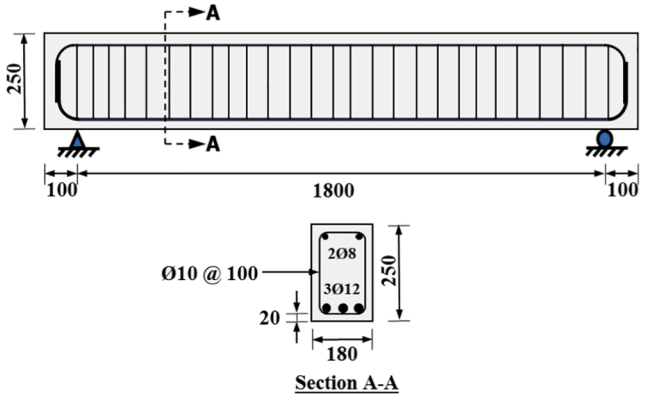

Fig. 2. The beams' geometrical and reinforcement details. All dimensions in mm.

respectively, while OPC was replaced at 20% by FA. GA were replaced with RCA using the direct volume replacement method, whereas both TWW and FA were incorporated by weight of fresh water and OPC, respectively. For all concrete mixes, GA and RCA were in the saturated surface dry (SSD) condition upon casting by immersing them in water for 24 h, followed by surface drying by a moistened cloth. In addition, 0.2% superplasticizer by cement weight was added to achieve a minimum slump of 80 mm. Immediately after casting, concrete slump was measured according to ASTM C143/C143M-15a provisions [29]. Moreover, concrete compressive strength was measured at 28 days using three cylinders (100 × 200 mm) following ASTM C39/C39M-20 provisions [30]. In addition, concrete flexural strength was determined by

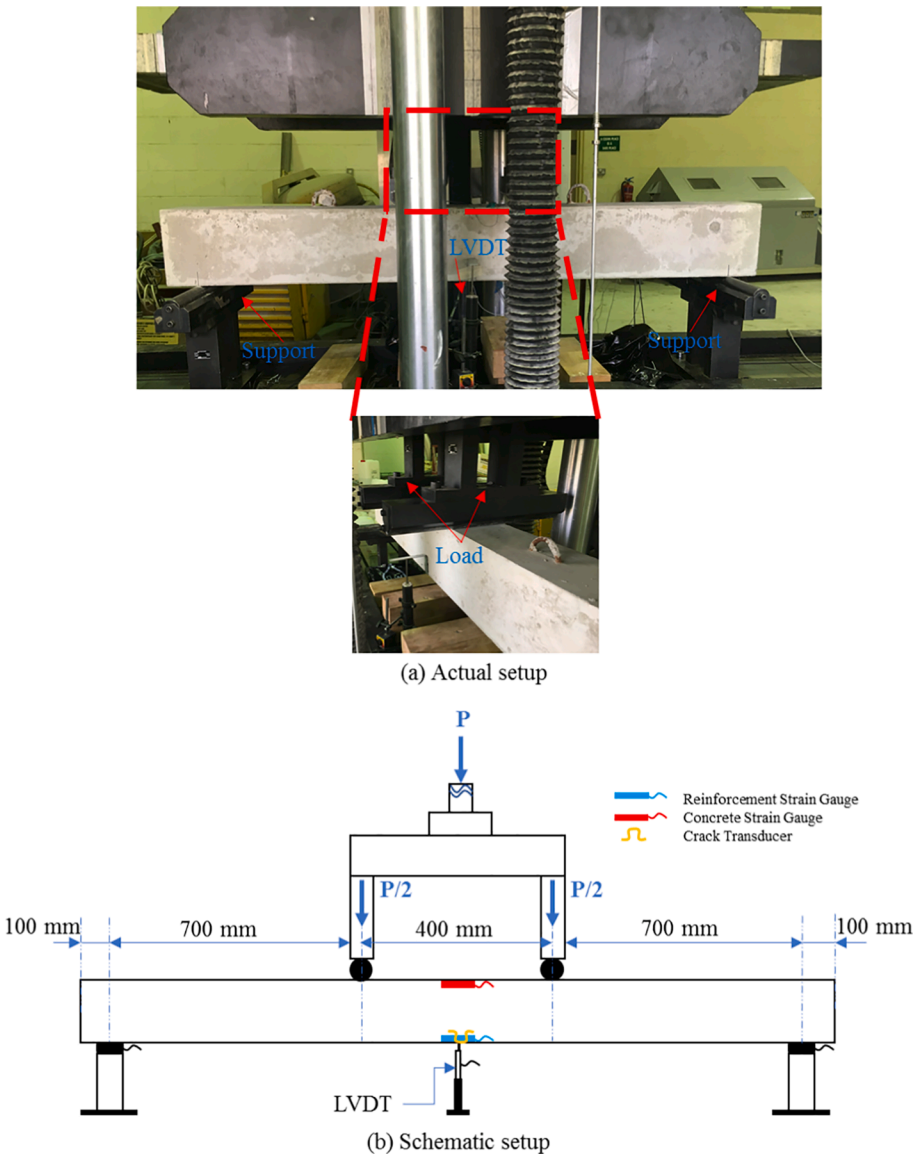

Fig. 3. Beam testing setup and instrumentations.

testing three prisms (100 × 100 × 500 mm) at 28 days according to ASTM C78/C78M-18 guidelines [31].

2.3. RC beam specimens

Four RC beams with dimensions of 180 × 250 × 2000 mm were prepared to evaluate the influence of TWW, RCA, and FA on the flexural behavior of RC beams. The only test variable considered in the tested beams was the concrete mix. The beams followed the same nomenclatures used for concrete mixes. That is, beams FGO, TGO, TRO, and TRF were prepared with concrete mixes FGO, TGO, TRO, and TRF, respectively. The beams' geometrical, reinforcement, and loading details are illustrated in Fig. 2. The beams' reinforcement was chosen to achieve a ductile-flexural failure mode as per ACI 318–19 design codes [32]. The beams were reinforced in the longitudinal direction with 3ϕ12 at the bottom and 2ϕ8 at the top. Moreover, the beams were reinforced in the transverse direction with ϕ10 steel stirrups spaced at 100 mm. A constant clear cover of 20 mm from all sides was maintained for all beams.

2.4. RC beam test setup

All beams were tested under a four-point bending setup until failure using a 1500-kN universal testing machine. The beams' setup and instrumentations are presented in Fig. 3. The beams were loaded under a displacement rate of 1 mm/min. For each beam, two concrete strain gauges were mounted at the compression mid-span to measure concrete strains. Moreover, two steel strain gauges were attached at the middle of the longitudinal tensile reinforcement before casting to record steel strains. In addition, two linear variable differential transducers (LVDTs) were placed at the midspans to record the maximum deflections. Furthermore, the crack widths were captured using a crack transducer placed at the tensile mid-span section. All instrumentations were linked to a data logger system, and the recording was performed at a rate of 1 reading per second. It is worth noting that the flexural test was stopped when the rapture of the first bar occurred.

Table 6
Concrete fresh and hardened mechanical properties.

Mix	Slump (mm)	Compressive strength (MPa)	Flexural tensile strength (MPa)
FGO	86	57.03	3.77
TGO	91	53.50	3.29
TRO	89	48.04	3.43
TRF	136	40.54	2.96

3. Results and discussion

3.1. Concrete mechanical properties

3.1.1. Slump

Concrete slump results are illustrated in Table 6. It could be observed from the results that mix TGO slightly varied by about 6% from the reference mix, implying that TWW has no significant effect on concrete workability. This might be attributed to the comparable suspended solids in TWW and fresh water, which resulted in achieving similar TWW concrete weight to that made with fresh water. It could also be noticed that the slump of mix TRO was only 2.2% lower than that of mix TGO. The slump of mix TRO was decreased insignificantly because GA and RCA were in SSD condition upon casting, and hence the water absorption and open pores of both aggregate types were unified. Alnahhal and Aljidda [13] also pointed out that utilizing RCA in the SSD condition resulted in no distinct discrepancy between the slump of RAC and NAC. Furthermore, mix TRF showed 53% higher slump than mix TRO, owing to the smaller size particle of FA, which decreased the friction between the binders and other ingredients. The enhancement in the slump of mix TRO could also be related to the reduced fresh hydration products of OPC, as the OPC content was decreased. Similar results were also observed by Alnahhal and Aljidda [13] and Lima et al. [19].

3.1.2. Compressive strength

According to the results in Table 6, mix TGO had a 6.1% lower compressive strength than mix FGO. This might have occurred due to the delayed hydration of C_3A and C_3S, caused by the high concentrations of zinc and phosphate in TWW. The drop in the compressive strength of concrete with TWW could also be ascribed to the high concentration of chloride of TWW compared to fresh water, which increased the susceptibility to salt crystallization. The salt crystals, in turn, increased concrete voids and degraded the interfacial transition zone (ITZ) of concrete. The results also revealed that the compressive strength of mix TRO was 10.2% lower than that of mix TGO. This is commonly linked to the adhered mortar on RCA, which developed more internal cracks and voids in the matrix and thus weakened the ITZ layers [1,9,14]. It should be noted that the reduction in the compressive strength was insignificant because the replacement of coarse aggregates was performed as per the direct volume replacement method, which ensures a constant volume of GA and RCA in 1 m^3 of concrete [13]. Furthermore, mix TRF recorded

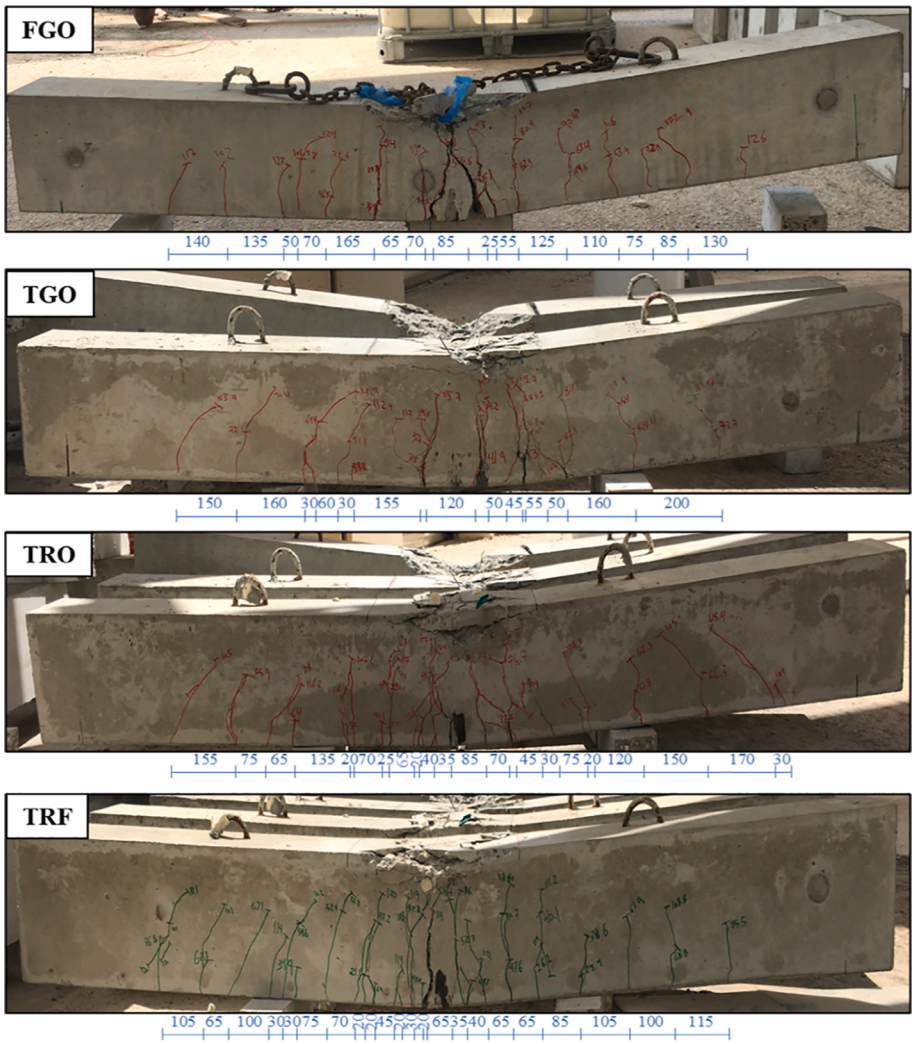

Fig. 4. Cracking patterns and failure modes of the beams (crack spacing is in mm).

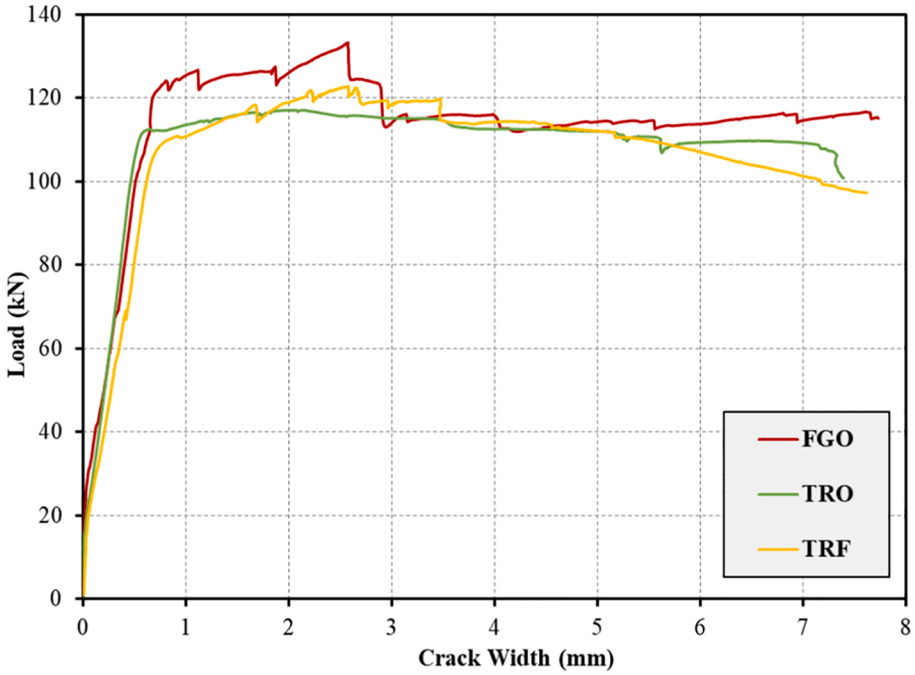

Fig. 5. Load-crack width responses of the beams.

15.6% lower compressive strength than TRO. That was because OPC content was reduced and thus decreased the hydration products of OPC. These observations are in line with results reported by Asadollahfardi et al. [6], Sunayana and Barai [20], and Anike et al. [33].

3.1.3. *Flexural tensile strength*

The flexural tensile strength of all concrete mixes at 28 days is presented in Table 6. Similar to the compressive strength results, prism TGO recorded 12.7% lower flexural tensile strength than prism FGO due to the high concentrations of zinc and phosphate in TWW. Besides, the results showed that RCA had no significant influence on the flexural tensile strength of concrete, as prism TRO recorded only 4.3% higher prism TGO. Moreover, it could be recognized that prism TRF achieved 13.7% lower flexural strength than prism TRO. This is attributed to the decreased OPC hydration products with the 20% reduction of OPC in mix TRF. The results obtained are in conformance with Alnahhal and Aljidda [13] and Abushanab and Alnahhal [14].

3.2. *Cracking patterns and failure modes*

The cracking patterns and failure modes of all tested beams are presented in Fig. 4. The cracking responses of the beams were captured during testing through a naked eye. It could be seen that all beams displayed a similar cracking pattern, regardless of concrete mix. That is, the first flexural crack in all beams was initiated within the flexural region at the early loading stage. With a further augmentation in the applied load, the cracks were widened and propagated vertically toward the compression side of the beam and additional cracks were developed in the shear zone.

As could be observed in Fig. 4, beam TGO recorded approximately similar cracking spacing to beam FGO. On the other hand, the crack spacing of beam TRO was closer than that of beams FGO and TGO. This is ascribed to residual mortar on RCA, which degraded the ITZ layers between the aggregates and cement matrix and thus weakened the aggregate interlocking and shear strength of the beams. It is to be emphasized that the weak ITZ layer of RAC implies that RCA have inferior durability properties compared to NA. Arezoumandi et al. [16], Sunayana and Barai [20], and Al Mahmoud et al. [34] also reported that RAC-RC beams exhibited closer crack spacing than NAC-RC beams. Likewise, beam TRF displayed closer crack spacing than beams FGO, TGO, and TRO. The closely spaced cracks in beam TRF are attributed to the reduced flexural strength of mix TRF. Furthermore, Fig. 5 shows that beam TRO recorded relatively comparable crack widths to beam FGO, whereas beam TRF recorded about 50% higher crack width at yielding than beam TRO. The increase in the crack widths of beam TRF before yielding is fundamentally ascribed to the decreased flexural strength of mix TRF relative to mixes FGO, TGO, and TRO. However, the crack width of beam TRF at failure was similar to beams FGO, TGO, and TRO, ascribable to the similar axial stiffness of all beams. The results are in conformance with the findings of Yoo et al. [35], who revealed that FA decreased the crack spacing and increased crack widths of the beams. It should be mentioned that the load-crack width response of beam TGO was excluded from Fig. 5 because the largest crack width did not occur at the crack transducer zone.

Likewise, varying cracking loads were recorded with different concrete mixes. As could be seen in Table 7, the first cracking load was in the order of beams TRO, TGO, TRF, and FGO, respectively. In particular, the use of TWW and RCA in beams TGO and TRO decreased the cracking

Table 7
loads, deflections, and ductility indices of the tested beams.

Beam ID	P_{cr} (kN)	$P_{L/360}$ (kN)	P_y (kN)	P_u (kN)	$P_{failure}$ (kN)	Δ_y(mm)	$\Delta_{failure}$(mm)	Ductility index
FGO	30	90.40	123.50	133.35	115.09	8.25	68.62	8.32
TGO	28	80.17	113.22	115.12	110.94	8.42	63.99	7.60
TRO	24	73.69	112.24	117.09	100.85	9.55	60.42	6.39
TRF	28	67.13	110.09	122.90	96.96	8.80	56.58	6.43

Note: P_{cr}, P_y, and P_u are the cracking, yielding, and ultimate loads, respectively.

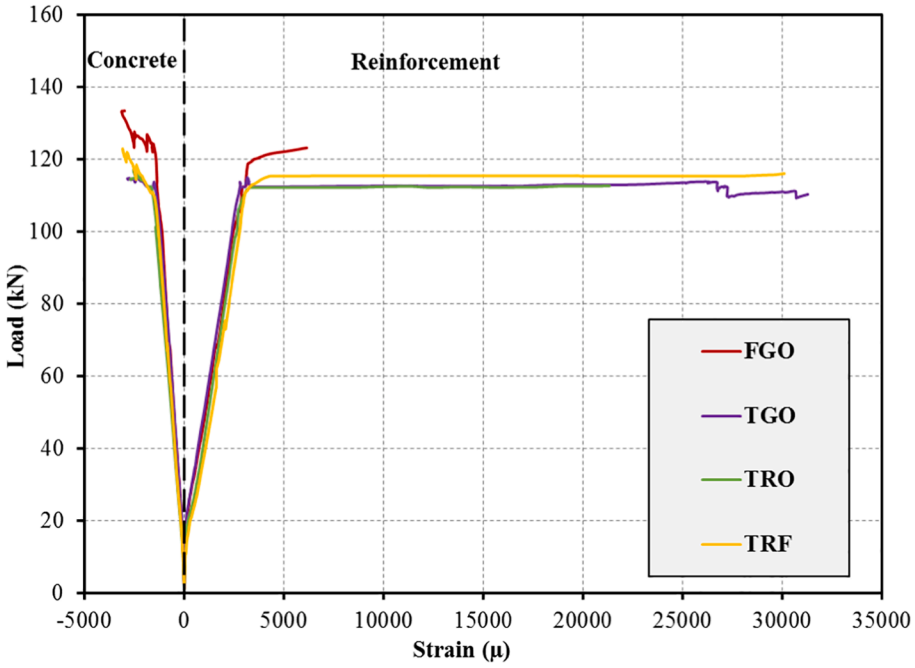

Fig. 6. Load-strain responses of the beams.

load by 6.7% and 14.3%, respectively. The drop in the cracking load of beams TGO and TRF compared to the reference beam is attributed to the decreased flexural strength of the mixes compared to mix FGO. On the other hand, beam TRF achieved 16.7% higher cracking load than beam TRO, owing to the pozzolanic reaction between FA and $Ca(OH)_2$, which densified the cement matrix and strengthened the weak ITZ layers. The obtained results are in line with Kang et al. [17].

Furthermore, the results indicated that the failure mode of the beams was independent of the concrete mix. All beams experienced a flexural tension failure mode, which started with the concrete cracking, followed by the tensile reinforcement yielding, and finally concrete crushing at the compression face. This was because the failure mode depends mainly on the reinforcement configuration, which was identical in all beams. This observation agrees with almost all studies of RCA and FA [13,16,20].

3.3. Load-strain response

The variation in concrete and reinforcement strains with respect to concrete mix is provided in Fig. 6. As depicted in the figure, all beams reported similar reinforcement and concrete strain responses with loading, regardless of concrete mix. Prior to cracking, concrete and tensile strains were relatively small and comparable in all beams. However, reinforcement strains upon cracking were significantly

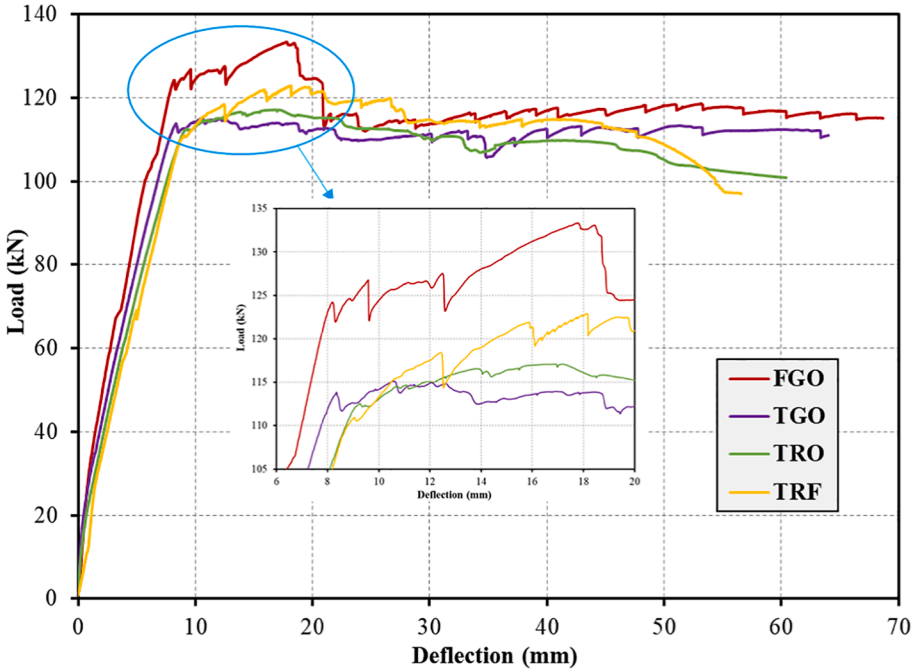

Fig. 7. Load-deflection responses of the beams.

Table 8
List of code-based expressions used to predict the cracking and ultimate moments and instantaneous deflections of conventional RC beams.

Cracking moment			
Design code	Moment capacity (N•mm)		Relevant formulas	
ACI 318–19 [32]	$M_{cr} = \frac{f_r I_g}{y_t}$ f_r = modulus rapture of concrete, (MPa) I_g = gross moment of inertia, (mm^4) y_t = distance from the centroid to the tensioned face, (mm)	(1)	$f_r = 0.62\lambda\sqrt{f_c'}\lambda$ = a modification factor = 1 (for normal-weight concrete) f_c' = concrete compressive strength, (MPa)	(2)
CSA-A23.3–14 [39]	$M_{cr} = \frac{f_r I_g}{y_t}$ f_r = modulus rapture of concrete, (MPa) I_g = gross moment of inertia, (mm^4) y_t = distance from the centroid to the tensioned face, (mm)	(3)	$f_r = 0.6\lambda\sqrt{f_c'}\lambda$ = a modification factor = 1 (for normal-density concrete) f_c' = concrete compressive strength, (MPa)	(4)
Eurocode 2 [40]	$M_{cr} = \frac{f_{ctm} I_u}{(h - X_u)}$ f_{ctm} = mean tensile strength of concrete, (MPa) I_u = moment inertia of uncracked section transformed to concrete, (mm^4) h = height of the cross-section X_u = neutral axis depth of uncracked section, (mm)	(5)	$f_{ctm} = 0.3 f_c'^{0.67}$	(6)
			$X_u = \frac{\frac{bh^2}{2} + (\alpha_e - 1)(A_s d + A_{s2} d_2)}{bh + (\alpha_e - 1)(A_s + A_{s2})}$	(7)
			$I_u = \frac{bh^3}{12} + bh\left(\frac{h}{2} - X_u\right)^2 + (\alpha_e - 1)\left[A_s(d - X_u)^2 + A_{s2}(X_u - d_2)^2\right]$	(8)
			α_e = a factor $= \frac{E_{steel}}{E_{concrete-effective}}$	(9)
			A_s = tensile steel reinforcement A_{s2} = compression steel reinforcement d = distance from extreme compression to tensile reinforcement d_2 = distance from extreme compression to compression reinforcement	
Ultimate moment As per the stress and strain distribution	$M_u = A_s f_y \left(d - \frac{a}{2}\right) + A_{s2} f_{s'} (d - d_2)$ A_s = tensile steel reinforcement (mm^2) A_{s2} = compression steel reinforcement (mm^2) d = distance from extreme compression to tensile reinforcement (mm) d_2 = distance from extreme compression to compression reinforcement (mm) f_y = yield strength of the tensile reinforcement (MPa) $f_{s'}$ = stress in the compression reinforcement (MPa) a = depth of the compressive block (mm)	(10)	$a = \frac{A_s f_y}{\alpha f_c' b}$ b = width of the beam α = a stress block parameter. The value of α can be calculated as follows: $\alpha = 0.85$ (ACI 318–19 [32]) $\alpha = 0.85 - 0.05\,(f_c' - 28)/7$(CSA-A23.3–14 [39])	(11) (12)
			$\alpha = \begin{cases} 1 where f_c' \le 50 \\ 1 - \frac{f_c' - 50}{200} where 50 \le f_c' \le 70 \end{cases}$ (Eurocode 2 [40])	(13) (14)
Instantaneous deflection	$\Delta i = \frac{Pa}{48 E_c I_e}(3L^2 - 4a^2)$ P = total applied load (N) a = shear span (mm) E_c = modulus of elasticity of concrete (MPa) I_e = effective moment of inertia (mm^4) L = effective length (mm)	(15)	$E_c = 4700\sqrt{f_c'}$(ACI 318–19 [32])	(16)
			$E_c = 4500\sqrt{f_c'}$(CSA-A23.3–14 [39])	(17)
			$I_e = \left(\frac{M_{cr}}{M_a}\right)^3 I_g + \left[1 - \left(\frac{M_{cr}}{M_a}\right)^3\right] I_{cr} \le I_g$(ACI 318–19 [32])	(18)
			$I_e = I_{cr} + (I_g - I_{cr})\left(\frac{M_{cr}}{M_a}\right)^3 \le I_g$(CAN/CSA-A23.3–14 [39])	(19)
			$I_{cr} = \frac{bx^3}{3} + (2n - 1)A_{s2}(x - d_2)^2 + nA_s(d - x)^2$ x = distance from the compression face of the beam to the neutral axis (mm)	(20)
			n = modular ratio $= \frac{E_s}{E_c}$ E_s = modulus of elasticity of steel (MPa)	(21)

developed with the applied load until yielding. After yielding, reinforcement strains were further increased with a negligible increment in the load, taking a bi-linear shape. However, concrete strains after cracking were sharply increased with loading until concrete crushing. It could be seen that all beams exhibited similar concrete and tensile strains at yielding, regardless of concrete mix. This was because reinforcement was identical in all beams. On the other hand, it could be seen that beam TRF recorded 12.2% higher compressive strain at failure than beam TRO, indicating that concrete mix TRF is more densified and has better bond strength with reinforcement compared to mix TRO. The results are supported by the experimental results of Alnahhal and Aljidda [13], Kang et al. [17], and Yoo et al. [35].

3.4. Load-deflection response

Fig. 7 presents how the load–deflection response of the beams was affected by the concrete mixes. A summary of service, yielding, ultimate, and failure loads with the corresponding deflections are presented in Table 7. It is worth noting that the service load refers to the load corresponding to the displacement under serviceability conditions, which was calculated according to ACI 318–19 design code [32] as L/360, where L is the effective length of the beam. Moreover, the ductility indices of all beams were calculated as the ratio between the failure and yielding deflections in accordance with ACI 363R-10 [36] and listed in Table 7. It could be seen in Fig. 7 that all beams responded with similar load–deflection behavior, regardless of concrete mix. Overall, the load–deflection response of all beams consisted of three stages: linear pre-cracking, linear post-cracking with reduced stiffness, and non-linear post-yielding with reduced stiffness.

As anticipated, Fig. 7 shows that the variation in the flexural capacity of beams TGO and FGO was in agreement with the compressive strength results. The service, yielding, ultimate, and failure loads of beam TGO were 11.4%, 8.3%, 13.7%, and 3.6% lower than those of beam FGO, respectively. In addition, at the service load of beam FGO (P = 90.40 kN), beam TGO recorded about 17.1% higher deflection than beam FGO. Moreover, beam TGO exhibited an 8.7% lower ductility index than beam FGO (Table 7). The drop in the flexural capacity and ductility with the use of TWW is ascribed to the high concentrations of zinc and phosphate

Table 9
Experimental and predicted cracking moments of the beams.

Beam		ACI 318–19 [32]		CSA-A23.3–14 [39]		Eurocode 2 [40]	
	$M_{cr.-Exp.}$ (kN•m)	$M_{cr.-Pred.}$ (kN•m)	$\frac{M_{cr.-Exp.}}{M_{cr.-Pred.}}$	$M_{cr.-Pred.}$ (kN•m)	$\frac{M_{cr.-Exp.}}{M_{cr.-Pred.}}$	$M_{cr.-Pred.}$ (kN•m)	$\frac{M_{cr.-Exp.}}{M_{cr.-Pred.}}$
FGO	10.50	8.78	1.20	8.50	1.24	11.56	0.91
TGO	9.80	8.50	1.15	8.23	1.19	11.15	0.88
TRO	8.40	8.06	1.04	7.80	1.08	10.50	0.80
TRF	9.80	7.40	1.32	7.16	1.37	9.56	1.03
Mean			1.18		1.22		0.90
SD			0.12		0.12		0.09
COV%			9.87		9.87		10.35

Note: $M_{cr.-Exp.}$ = experimental cracking moment, $M_{cr.-Pred.}$ = predicted cracking moment, SD = standard deviation, and COV = coefficient of variance.

in TWW, which delayed the hydration of C_3A and consequently decreased the compressive strength of concrete. On the other hand, it could be observed from Table 7 that there was no significant difference between beams FGO and TGO in terms of yielding and failure deflections. This was expected since deflection at yielding and failure stages depends mainly on reinforcement properties and configuration, which were the same in all beams.

Furthermore, it could be noticed that the flexural stiffness of the beams was slightly decreased after cracking when GA was replaced with RCA. Even though beams TGO and TRO exhibited comparable ultimate loads, beam TRO recorded 8.1% and 9.1% lower service and failure loads than beam TGO, respectively. Moreover, beam TRO presented 11.9% and 5.6% smaller deflection at failure than beams FGO and TGO, respectively. In addition, the results revealed that the ductility index of beam TRO was 15.9% lower than that of beam TGO, indicating that the brittleness of the beams increased with RCA. The decreased service and failure loads and ductility of RAC beams is attributed to residual mortar on RCA, which developed multiple ITZ layers in concrete matrix and consequently reduced the modulus of elasticity of RAC [9,13]. It was also observed that the yielding and ultimate loads of beams TRO and TGO were comparable, indicating that the yielding and ultimate loads depend mainly on the properties and configuration of steel reinforcement.

Meanwhile, it could be recognized from Fig. 7 that beam TRF had approximately a similar load–deflection response to that of beam TRO before yielding. However, the results showed that beam TRF achieved higher flexural capacity than beam TRO. Whereas beams TRO and TRF recorded comparable yielding and failure loads, beam TRF recorded 6.8% and 4.9% higher ultimate load than beams TGO and TRO, respectively. Furthermore, beam TRF exhibited 6.4% lower deflection at failure than beam TRO. In addition, the ductility of beam TRF was negligibly increased (<1%) compared to that of beam TRO. The higher flexural capacity and ductility with the addition of FA might be explained by the pozzolanic reaction between FA and $Ca(OH)_2$, which produced C—S—H gel and consequently densified the cement matrix and improved the cohesion between concrete and reinforcement. The improvement observed in beam TRF could also be related to the small-size particle of FA, which penetrated the aggregate-cement matrix interface and coated RCA, and accordingly improved the interlocking of RCA. Yoo et al. [35] and Hashmi and Baqi [37] also observed that the partial replacement of OPC with FA enhanced the load–deflection response and ductility of the beams.

Moreover, it is to be emphasized that in seismic design provisions, structural ductility plays a significant role in achieving an earthquake-resilient design. That is, structures with sufficient ductility are ensured to remain intact during minor earthquakes, minorly damaged during moderate earthquakes, and partially damaged with no collapse during major earthquakes [38]. However, as presented above, ductility marginally. Though, the results demonstrated that FA improved the beams' ductility. Thus, it is anticipated that FA could improve the earthquake resistance of the TWW and RCA concrete structures.

4. Code provisions

The available design-guideline equations have not yet addressed the effect of TWW, RCA, and FA on the flexural capacity and deflection of simply supported RC beams. Therefore, to address the approximation degree of the available design-code expressions to the tested RC beams, a comprehensive comparison between the experimental and predicted results in terms of cracking and ultimate moments and instantaneous deflections was performed in this study. The design-code equations to predict the cracking and ultimate moments and load–deflection responses are summarized in Table 8.

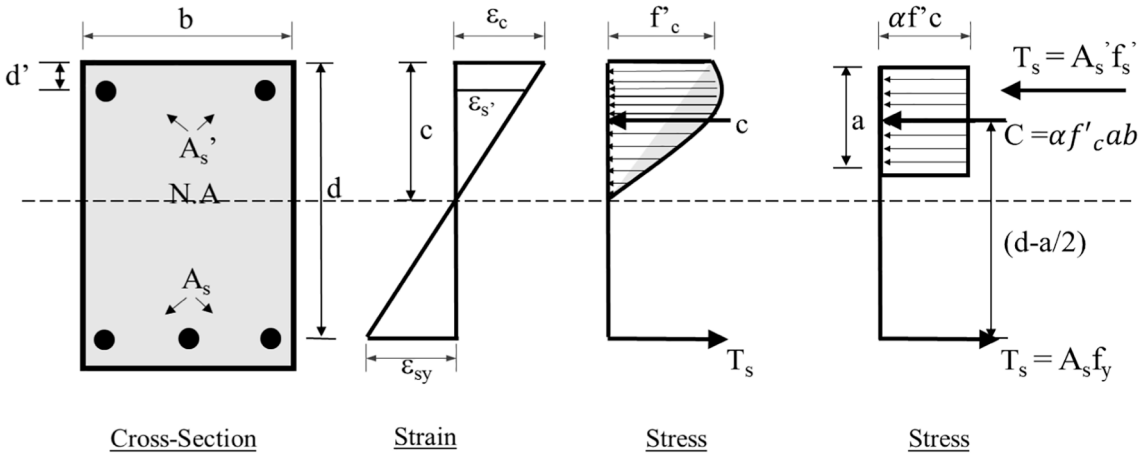

Fig. 8. Distribution of stresses and strains for a typical RC beam.

Table 10
Experimental and predicted ultimate moments of the beams.

Beam		ACI 318–19 [32]		CSA-A23.3–14 [39]		Eurocode 2 [40]	
	$M_{u-Exp.}$ (kN•m)	$M_{u-Pred.}$ (kN•m)	$\frac{M_{u-Exp.}}{M_{u-Pred.}}$	$M_{u-Pred.}$ (kN•m)	$\frac{M_{u-Exp.}}{M_{u-Pred.}}$	$M_{u-Pred.}$ (kN•m))	$\frac{M_{u-Exp.}}{M_{u-Pred.}}$
FGO	46.67	45.80	1.02	45.21	1.04	46.02	1.03
TGO	40.29	45.68	0.89	45.15	0.90	45.94	0.89
TRO	40.98	45.46	0.91	45.02	0.92	45.78	0.91
TRF	43.02	45.06	0.96	44.76	0.97	45.45	0.96
Mean			0.95		0.96		0.94
SD			0.06		0.06		0.06
COV%			6.54		6.61		6.59

Note: $M_{u-Exp.}$ = experimental ultimate moment and $Mu_{-Pred.}$ = predicted ultimate moment.

4.1. Cracking moment

The cracking moment (M_{cr}) of the tested beams was computed using the design-code equations of ACI 318–19 [32], CSA-A23.3–142 [39], and Eurocode 2 [40] (Eqs. (1) to (9)). The experimental-to-predicted cracking moment ($M_{cr\text{-}Exp.}/M_{cr\text{-}Pred}$) ratios are listed in Table 9. As could be noticed, the $M_{cr\text{-}Exp.}/M_{cr\text{-}Pred.}$ ratios of beams FGO, TGO, and TRO were within the range of 1 ± 0.20, except for the CSA-A23.3–142 [39] prediction of beam FGO, which exhibited an $M_{cr\text{-}Exp.}/M_{cr\text{-}Pred}$ ratio of 1.24. On the other hand, it could be seen that ACI 318–19 [32] and CSA-A23.3–142 [39] provisions significantly underestimated the cracking moment of beam TRF with $M_{cr\text{-}Exp.}/M_{cr\text{-}Pred}$ ratios of 1.32 and 1.37, respectively. The excessive over conservation of beam TRF is related to the influence of FA in enhancing the cracking load, which was not considered in any of the guidelines. However, Eurocode 2 [40] guidelines showed a less conservative prediction for beam TRF with an $M_{cr\text{-}Exp.}/M_{cr\text{-}Pred}$ ratio of 1.03. This might have occurred because the tensile strength of concrete calculated by Eurocode 2 [40] was higher than those calculated by ACI 318–19 [32] and CSA-A23.3–142 [39] provisions (see Eqs. (2), (4), and (6)), and hence Eurocode 2 [40]

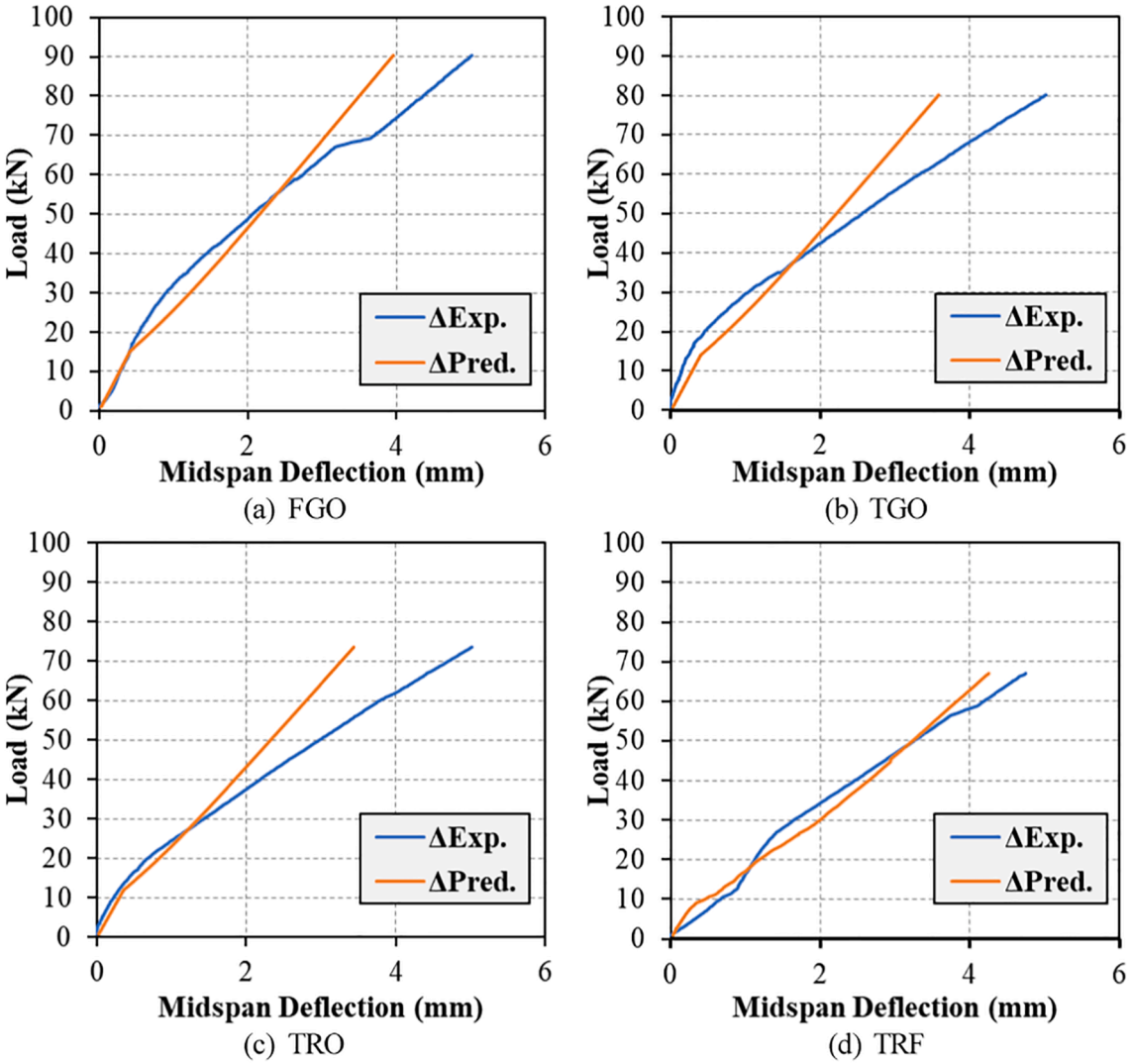

Fig. 9. Experimental and predicted load–deflection responses as per ACI 318–19 [32].

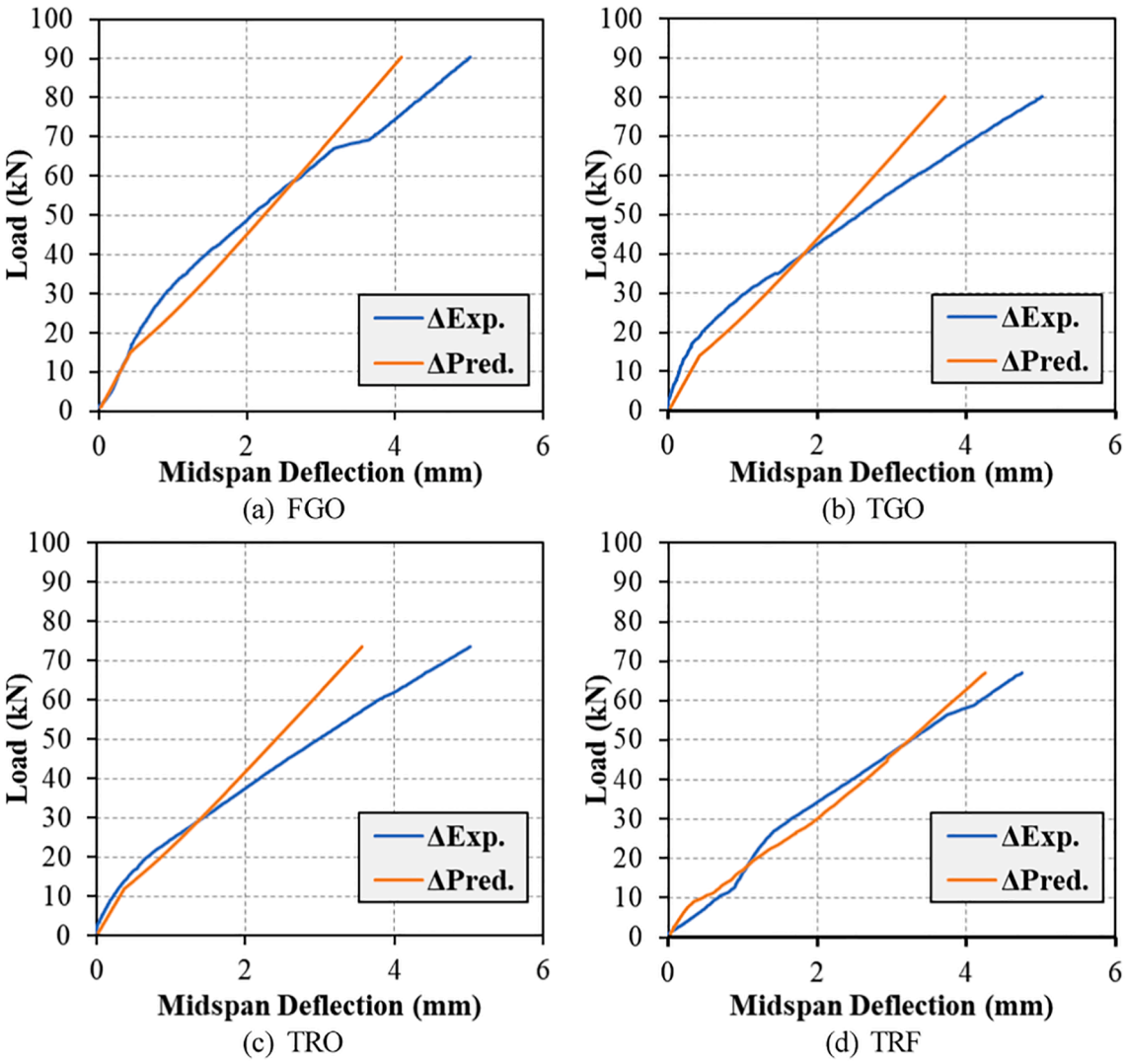

Fig. 10. Experimental and predicted load–deflection responses as per CSA-A23.3–14 [39].

exhibited higher cracking moment than ACI 318–19 [32] and CSA-A23.3–142 [39]. Even though the cracking moment of beam TRF was accurately predicted by Eurocode 2 [40], the overall prediction of Eurocode 2 [40] was unconservative, as it recorded an $M_{cr\text{-}Exp.}/M_{cr\text{-}Pred}$ ratio of 0.9. By contrast, the overall prediction of ACI 318–19 [32] and CSA-A23.3–142 [39] provisions was conservative and safe, and, in particular, ACI 318–19 [32] exhibited the most accurate prediction of the cracking moment for the tested beams with a mean, standard deviation (SD), and coefficient of variance (COV) $M_{cr\text{-}Exp.}/M_{cr\text{-}Pred.}$ ratio of 1.18, 0.12, and 9.87%, respectively.

4.2. Ultimate moment

The ultimate moment capacity (M_u) of the tested beams was calculated considering the stress and strain distribution approach as per ACI 318–19 [32], CSA-A23.3–142 [39], and Eurocode 2 [40] provisions. The distribution of stresses and strains of a typical RC beam under flexure is presented in Fig. 8. A shown in Fig. 8, the width of the compression stress block is represented by $\alpha f_c^{'}$, where α is the stress block parameter and $f_c^{'}$ is the compressive strength of concrete. Based on the distribution presented in Fig. 8, the M_u can be calculated using Eq. (10) (see Table 8). In addition, the value of α can be calculated using Eqs. (12), (13), and (14) as per ACI 318–19 [32], CSA-A23.3–142 [39], and Eurocode 2 [40] provisions, respectively. For each expression of α, the ratio of the experimental-to-predicted ultimate moment capacity ($M_{u\text{-}Exp.}/M_{u\text{-}Pred.}$) was calculated and listed in Table 10. It could be seen that ACI 318–19 [32], CSA-A23.3–142 [39], and Eurocode 2 [40] provisions provided accurate M_u prediction for beam FGO with $M_{u\text{-}Exp.}/M_{u\text{-}Pred.}$ ratios of 1.02, 1.04, and 1.03 , respectively. Nonetheless, the M_u of beams TGO, TRO, and TRF was slightly overestimated by all design codes. Overall, all design codes yielded unconservative predictions for M_u with $M_{u\text{-}Exp.}/M_{u\text{-}Pred.}$ ratios 0.94 to 0.96. The overestimation of the beams' flexural capacities might be because the available design codes have not yet included the influence of TWW, RCA, and FA. In this work, the least prediction error for the M_u was for CSA-A23.3–142 [39] with a mean, SD, and COV $M_{u\text{-}Exp.}/M_{u\text{-}Pred.}$ ratio of 0.96, 0.06, and 6.61%, respectively.

4.3. Load-deflection response

The theoretical load–deflection responses of the tested beams were calculated up to the service load as per ACI 318–19 [32] and CSA-A23.3–142 [39] provisions using Eqs. (15) to (21). Prior to cracking, the beams were assumed to have a gross moment of inertia (I_g). However, upon cracking, the I_g is gradually decreased to the cracking moment of inertia (I_{cr}). To account for the transition between the I_g and I_{cr}, the effective moment of inertia (I_e) was calculated using Eqs. (18) and (19) as per ACI 318–19 [32] and CSA-A23.3–142 [39] provisions, respectively. The theoretical load–deflection responses predicted by ACI

318–19 [32] and CSA-A23.3–142 [39] provisions are compared to the experimental ones in Fig. 9 and Fig. 10, respectively. The analysis showed the predicted load–deflection responses by ACI 318–19 [32] and CSA-A23.3–142 [39] provisions were overall congruent with the experimental responses, except for the maximum deflection, which was slightly underestimated by both provisions. CSA-A23.3–142 [39] was marginally less conservative and more accurate than ACI 318–19 [32] in predicting the maximum deflection, suggesting that CSA-A23.3–142 [39] is more applicable in predicting the maximum deflection RC beams made with TWW, RCA, and FA.

5. Conclusions

This study presented experimental and analytical investigations on the flexural behavior of RC beams made with TWW, RCA, and FA. Four concrete mixes using different mixing water types (fresh water and TWW), coarse aggregate types (GA and RCA), and FA replacement ratios (0% and 20%) were investigated. In addition, four RC beams made from the four concrete mixes were prepared and tested under a four-point bend flexure until failure. The study's findings are summarized in the following points:

1- The use of TWW and RCA showed no significant influence on concrete slump. However, replacing 20% of OPC with FA increased concrete slump by 53%. In addition, the compressive strength of concrete was reduced by 6 to 16% when TWW, RCA, and FA were used. Furthermore, TWW and FA decreased concrete flexural tensile strength by about 13%, whilst RCA showed no significant effect on concrete flexural strength.
2- The use of TWW demonstrated no effect on the number and spacing of cracks. Nevertheless, the use of FA and RCA resulted in a higher number of closely spaced cracks. Moreover, the cracking loads were decreased by 6.7% and 14.3% when TWW and RCA were used, respectively. Conversely, the addition of FA increased the cracking loads by 16.7%. Furthermore, the beams' crack widths and failure mode were not influenced by the concrete mix. In addition, FA increased the maximum compressive strain by 12.2%.
3- TWW decreased the service, yielding, ultimate, and failure loads by 11.4%, 8.3%, 13.7%, and 3.6%, respectively, and increased the mid-span deflection by 17.1%. Furthermore, TWW decreased the beams' ductility by 8.7%. Likewise, RCA decreased the service and failure loads and ductility of the beams by 8.1%, 9.1%, and 15.9%, respectively. On the other hand, FA decreased the deflections at yielding and failure by 7.9% and 6.4%, respectively, and negligibly enhanced the beams' ductility.
4- The obtained results were analytically compared with the available design-guideline equations. The most accurate prediction of the cracking moments was governed by ACI 318–19, whilst CSA-A23.3–14 showed the least prediction error for the beams' ultimate moments. In addition, CSA-A23.3–14 yielded the most accurate prediction of the beams' load–deflection responses.

Finally, it should be mentioned that the results obtained from this study are based solely on the characteristics of the TWW, RCA, and FA used. Accordingly, further studies should be performed to confirm the obtained results and to address the influence of TWW, RCA, and FA in the available analytical formulations in order to accurately predict the beams' flexural capacities. It is also recommended to investigate the long-term durability of RC beams with TWW, RCA, and FA

Declaration of Competing Interest

The authors declare that they have no known competing financial interests or personal relationships that could have appeared to influence the work reported in this paper.

Acknowledgment

This publication was made possible by GSRA grant GSRA6-1-0509-19022 from the Qatar National Research Fund (QNRF, a member of Qatar Foundation). The authors would like also to thank the Central Laboratories Unit (CLU) at Qatar University for the chemical characteristics of treated wastewater. Also, the financial support from Qatar University through grant no. QUST-1-CENG-2021-20 is acknowledged. The findings achieved herein are solely the responsibility of the authors.

References

[1] Abushanab A, Alnahhal W, Sohail MG, Alnuaimi N, Kahraman R, Altayeh N. Mechanical and durability properties of ultra-high performance steel FRC made with discarded materials. J. Build. Eng. 2021;44:103264. https://doi.org/10.1016/j.jobe.2021.103264.
[2] Abushanab A, Alnahhal W. Combined effects of treated domestic wastewater, fly ash, and calcium nitrite toward concrete sustainability. J. Build. Eng. 2021;44:103240. https://doi.org/10.1016/j.jobe.2021.103240.
[3] Alnahhal W, Taha R, Alnuaimi N, Al-Hamrani A. Properties of fibre reinforced concrete made with discarded materials. Mag. Concr. Res. 2018;71:1–38. https://doi.org/10.1680/jmacr.17.00293.
[4] Arooj MF, Haseeb F, Butt AI, Irfan-Ul-Hassan DM, Batool H, Kibria S, et al. A sustainable approach to reuse of treated domestic wastewater in construction incorporating admixtures. J. Build. Eng. 2021;33:101616.
[5] Shekarchi M, Yazdian M, Mehrdadi N. Use of biologically treated domestic waste water in concrete. Kuwait J. Sci. Eng. 2012;39:97–111.
[6] Asadollahfardi G, Delnavaz M, Rashnoiee V, Ghonabadi N. Use of treated domestic wastewater before chlorination to produce and cure concrete. Constr. Build. Mater. 2016;105:253–61. https://doi.org/10.1016/j.conbuildmat.2015.12.039.
[7] Abushanab A, Alnahhal W. Characteristics of Concrete Made with Treated Domestic Wastewater. In: Kang T, Lee Y, editors., Singapore: Springer Singapore; 2022, p. 231–5. https://doi.org/10.1007/978-981-16-6932-3_20.
[8] Mohammed SI, Najim KB. Mechanical strength, flexural behavior and fracture energy of Recycled Concrete Aggregate self-compacting concrete. Structures 2020;23:34–43. https://doi.org/10.1016/j.istruc.2019.09.010.
[9] Wang Y, Hughes P, Niu H, Fan Y. A new method to improve the properties of recycled aggregate concrete: Composite addition of basalt fiber and nano-silica. J. Clean. Prod. 2019;236:117602. https://doi.org/10.1016/j.jclepro.2019.07.077.
[10] Kisku N, Rajhans P, Panda SK, Pandey V, Nayak S. Microstructural investigation of recycled aggregate concrete produced by adopting equal mortar volume method along with two stage mixing approach. Structures 2020;24:742–53. https://doi.org/10.1016/j.istruc.2020.01.044.
[11] Hossain MU, Poon CS, Lo IMC, Cheng JCP. Comparative environmental evaluation of aggregate production from recycled waste materials and virgin sources by LCA. Resour. Conserv. Recycl. 2016;109:67–77. https://doi.org/10.1016/j.resconrec.2016.02.009.
[12] Chen J, Wang Y, Roeder CW, Ma J. Behavior of normal-strength recycled aggregate concrete filled steel tubes under combined loading. Eng. Struct. 2017;130:23–40. https://doi.org/10.1016/j.engstruct.2016.09.046.
[13] Alnahhal W, Aljidda O. Flexural behavior of basalt fiber reinforced concrete beams with recycled concrete coarse aggregates. Constr. Build. Mater. 2018;169:165–78. https://doi.org/10.1016/j.conbuildmat.2018.02.135.
[14] Abushanab A, Alnahhal W. Performance of sustainable concrete incorporating treated domestic wastewater, RCA, and fly ash. Constr. Build. Mater. 2022;329:127118. https://doi.org/10.1016/j.conbuildmat.2022.127118.
[15] Choi W-C, Yun H-D. Long-term deflection and flexural behavior of reinforced concrete beams with recycled aggregate. Mater. Des. 2013;51:742–50. https://doi.org/10.1016/j.matdes.2013.04.044.
[16] Arezoumandi M, Smith A, Volz JS, Khayat KH. An experimental study on flexural strength of reinforced concrete beams with 100% recycled concrete aggregate. Eng. Struct. 2015;88:154–62. https://doi.org/10.1016/j.engstruct.2015.01.043.
[17] Kang T-H-K, Kim W, Kwak Y-K, Hong S-G. Flexural Testing of Reinforced Concrete Beams with Recycled Concrete Aggregates. ACI Struct. J. 2014;111. https://doi.org/10.14359/51686622.
[18] Seara-Paz S, González-Fonteboa B, Martínez-Abella F, Eiras-López J. Flexural performance of reinforced concrete beams made with recycled concrete coarse aggregate. Eng. Struct. 2018;156:32–45. https://doi.org/10.1016/j.engstruct.2017.11.015.
[19] Lima C, Caggiano A, Faella C, Martinelli E, Pepe M, Realfonzo R. Physical properties and mechanical behaviour of concrete made with recycled aggregates and fly ash. Constr. Build. Mater. 2013;47:547–59. https://doi.org/10.1016/j.conbuildmat.2013.04.051.
[20] Sunayana S, Barai SV. Flexural performance and tension-stiffening evaluation of reinforced concrete beam incorporating recycled aggregate and fly ash. Constr. Build. Mater. 2018;174:210–23. https://doi.org/10.1016/j.conbuildmat.2018.04.072.
[21] Association APH. Standard Methods for the Examination of Water and Wastewater. 22st ed. Washington DC, USA: American Public Health Association; 2012.
[22] Qcs Qatar General Organization for Standards and Metrology 2014 Qatar.

[23] Astm 1602, c1602m,. – 18. Standard Specification for Mixing Water Used in the Production of Hydraulic Cement. Concrete 2018. https://doi.org/10.1520/C1602_C1602M-18.
[24] Bs:en:1008:2002.. Mixing water for concrete: specification for sampling, testing and assessing the suitability of water, including water recovered from processes in the concrete industry as mixing water for concrete. Br Stand Inst 2002.
[25] ASTM C33/C33M – 18. Standard Specification for Concrete Aggregates. 2018. https://doi.org/10.1520/C0033_C0033M-18.
[26] ASTM C311 / C311M – 18. Standard Test Methods for Sampling and Testing Fly Ash or Natural Pozzolans for Use in Portland-Cement Concrete. 2018. https://doi.org/10.1520/C0311_C0311M-18.
[27] ASTM C150/C150M – 20. Standard Specification for Portland Cement. 2020. https://doi.org/10.1520/C0150_C0150M-20.
[28] Astm. C618–19. Standard Specification for Coal Fly Ash and Raw or Calcined Natural Pozzolan for Use in. Concrete 2019. https://doi.org/10.1520/C0618-19.
[29] Standard Test Method for Slump of Hydraulic-Cement Concrete. ASTM C143/C143M-15a 2015:15–8. https://doi.org/10.1520/C0143_C0143M-15A.
[30] Standard Test Method for Compressive Strength of Cylindrical Concrete Specimens. ASTM C39/C39M-20 2020:1–8. https://doi.org/10.1520/C0039_C0039M-20.
[31] ASTM C78/C78M – 18. Standard Test Method for Flexural Strength of Concrete (Using Simple Beam with Third-Point Loading). 2018. https://doi.org/10.1520/C0078_C0078M-18.
[32] (ACI Comm 2019:318–39.
[33] Anike EE, Saidani M, Olubanwo AO, Anya UC. Flexural performance of reinforced concrete beams with recycled aggregates and steel fibres. Structures 2022;39:1264–78. https://doi.org/10.1016/j.istruc.2022.03.089.
[34] Al Mahmoud F, Boissiere R, Mercier C, Khelil A. Shear behavior of reinforced concrete beams made from recycled coarse and fine aggregates. Structures 2020;25:660–9. https://doi.org/10.1016/j.istruc.2020.03.015.
[35] Yoo S-W, Ryu G-S, Choo JF. Evaluation of the effects of high-volume fly ash on the flexural behavior of reinforced concrete beams. Constr. Build. Mater. 2015;93:1132–44. https://doi.org/10.1016/j.conbuildmat.2015.05.021.
[36] ACI Committee 363. State-of-the-Art Report on High-Strength Concrete. vol. 92. 1997.
[37] Fuzail Hashmi A, Shariq M, Baqi A. Flexural performance of high volume fly ash reinforced concrete beams and slabs. Structures 2020;25:868–80. https://doi.org/10.1016/j.istruc.2020.03.071.
[38] Rodrigues H, Elawady MH. Ductility considerations in seismic design of reinforced concrete frame buildings according to the Eurocode 8. Innov Infrastruct Solut 2019;4:6. https://doi.org/10.1007/s41062-018-0192-x.
[39] Canadian Standards Association. Design of concrete structures (CAN/CSA-A23.3-14). Toronto, Ontario, Canada: Canadian Standards Association; 2014.
[40] Standard B. Eurocode 2: Design of concrete structures—. Part 1-1 Gen Rules Rules Build 2004:230.